Impurity effects on the electronic structure of square quantum dots: A full configuration-interaction study

Bhalchandra S. Pujari,[1,2,*] Kavita Joshi,[2] D. G. Kanhere,[1,2] and S. A. Blundell[3]

[1]*Department of Physics, University of Pune, Ganeshkhind, Pune 411 007, India*
[2]*Center for Modeling and Simulation, University of Pune, Ganeshkhind, Pune 411 007, India*
[3]*Service de Physique Statistique, Magnétisme et Supraconductivité, INAC, CEA-Grenoble/DSM, 17 rue des Martyrs,
F-38054 Grenoble Cedex 9, France*

We perform a full configuration-interaction study on a square quantum dot containing several electrons in the presence of an attractive impurity. The magnetic ordering in the dot is analyzed using appropriate pair-correlation functions. We find that a change in the size of the quantum dot can change the nature of the impurity from nonmagnetic to magnetic. In the low-density regime, the impurity traps one electron and the magnetic moment on the localized peaks outside the impurity fluctuates from negative to positive going through zero as a function of number of electrons. We also observe that the impurity changes the charge densities of excited states of two-electron quantum dot significantly, which in the absence of the impurity are almost similar. Our study also shows that in the strongly correlated regime the configuration-interaction approach yields ~20% more localization than density-functional theory. It has also been observed that only a small fraction of the total number of Slater determinants are required to produce ~99% of the converged charge density.

PACS number(s): 73.21.La, 71.55.−i, 71.27.+a, 31.15.V−

I. INTRODUCTION

Modern day technology has enabled us to fabricate nanoscopic devices in which electrons are confined by means of an external electrostatic field in a tiny island. Such artificially confined electrons are called *quantum dots*. The number of electrons in these *artificial atoms* is highly tunable.[1–4] The external confining potential can also be designed at will.[3] The parabolic potential is the most commonly considered model theoretically, but a square well, a triangular well, and other potentials have also been used routinely.[3,5–7] In the present work we consider the external confining potential to be a square well, where confinement effects influenced by the geometry are rather prominent. Square quantum dots have been analyzed by several authors.[3,7–9] For an extensive review on quantum dots, we refer the reader to Refs. 2 and 3.

Quantum dots have been studied theoretically by various methods such as spin-density-functional theory (SDFT),[3,5,7–12] quantum Monte Carlo (QMC),[13,14] coupled cluster,[15,16] and configuration interaction (CI).[3,17–20] The SDFT has proven successful in treating a variety of many-body problems including quantum dots.[18] The SDFT enables one to handle large systems with considerable ease. However, the SDFT, having the form of a mean-field theory, is known to have some limitations, such as broken symmetry.[9,11,12]

The CI method, on the other hand, provides a numerically highly accurate solution to the many-body Schrödinger equation.[21] The CI method is extensively used in electronic structure calculations, especially in quantum chemistry. Although the CI is computationally expensive, it has proved to be invaluable in probing the effects of electron-electron correlations especially for systems having small number of electrons (<10). For larger systems methods based on density-functional theory (DFT) are the obvious choice, but for smaller systems the assessment of the results of such methods by CI is always warranted.

The effect of various impurities on the properties of quantum dots has been a subject of interest in the recent years.[9,22–26] Our earlier study[9] has brought out the effect of an attractive impurity on the electronic structure of the quantum dots. The study was carried out using SDFT for a dot containing from 2 to 20 electrons with a wide range of dot sizes. It was observed that the impurity induces a localized magnetic moment that in many cases generates spin-polarized configurations with an antiferromagnetic coupling. Reusch and Egger[26] have used path-integral Monte Carlo to study the effect of an impurity on quantum dots near the Wigner molecule regime. Räsänen *et al.*[22] have studied the effect of an impurity placed in the vicinity of a quantum dot on the single-electron-transport spectrum. They have observed that the impurity evens out the state alternation as a function of magnetic field. The electronic structure of a spherical quantum dot with an impurity has been studied by Şahin and Tomak.[23] They have found that the capacitive energy increases in the presence of an impurity. Studies of an off-center hydrogenic impurity have been carried out by Movilla and Planelles.[24]

It is well known that in the low-density regime the correlations are crucial. A recent study by Ghosal *et al.*[14] has demonstrated the correlation-induced inhomogeneity in the electronic structure of the quantum dots. Our earlier work[9] was carried out with SDFT and it is necessary to test those results using a many-body technique. In the present work we apply the full CI method on a square quantum dot containing up to six electrons in the presence of a central attractive impurity. Our correlation analysis shows that upon increase in the size of the dot the central impurity changes its nature from nonmagnetic to magnetic. We also study extensively the nature of excited states of two-electron quantum dot and

the effects of impurity on the same. We also compare the CI results with SDFT wherever applicable where we find that the SDFT does produce qualitatively correct results.

The paper is organized as follows. In Sec. II, we describe the computational techniques used in the paper. Section III A describes the properties of the quantum dot without an impurity, including the excited states of the dot as well as the ground-state properties. The effect of an impurity is discussed in Sec. III B in a similar manner. We conclude in Sec. IV.

II. COMPUTATIONAL DETAILS

The quantum dot is modeled as N interacting electrons confined in an external confining potential. The dot is assumed to be quasi-two-dimensional. For such a system the Hamiltonian can be written in the effective-mass approximation as[3]

$$H = \sum_{i=1}^{N} \left[-\frac{(\hbar \nabla_i)^2}{2m^*} + V_{\text{ext}}(\mathbf{r}_i) \right] + \sum_{i<j} \frac{e^2}{4\pi\epsilon\epsilon_0 |\mathbf{r}_i - \mathbf{r}_j|}. \quad (1)$$

For a GaAs quantum dot the effective mass $m^* = 0.067 m_e$ and the dielectric constant $\epsilon = 12.4$. The length is expressed in the effective Bohr radius $a_0^* = 9.7$ nm and the energy is given in effective hartree, 1 Ha$^* = 11.9$ meV.

The confining potential is modeled as a square well with hard walls and is of the form

$$V_{\text{ext}}(x,y) = \begin{cases} 0, & 0 \geq x \geq L; \ 0 \geq y \geq L \\ V_0, & \text{otherwise,} \end{cases} \quad (2)$$

where L is the length of the quantum dot and the barrier height $V_0 = 100$ Ha*. In the case of a dot with an impurity, we also add to the Hamiltonian the impurity potential, which has the form

$$V_{\text{imp}}(x,y) = -A e^{-\beta(x^2+y^2)}, \quad (3)$$

where A is set to 8 Ha*, $1/\beta = 1.182 a_0^{*2}$, and the width of the impurity is $\sim 1.5 a_0^*$. The parameters for the impurity remain unchanged irrespective of the size of the dot. These parameters have been adjusted in such a way that for the single-electron case it only contains one bound state. While the width of the impurity is generally too large for a single atomic impurity, it enables us to study explicitly the role of many-body effects on the magnetic behavior. It should be noted that we do not assume an effective magnetic impurity by adding a Heisenberg-type term $J\mathbf{S}\cdot\boldsymbol{\mu}$ to the Hamiltonian (where $\mathbf{S}$ is the electron spin and $\boldsymbol{\mu}$ is the spin of the impurity). Rather, we add an attractive well explicitly and determine the resulting magnetic properties by a many-body calculation.

The size of the dot determines the density parameter r_s, with respect to which all the physical parameters are calculated and which is defined as

$$r_s = L \sqrt{\frac{1}{\pi N}}. \quad (4)$$

It is an approximate average Wigner-Seitz radius calculated by assuming the electron density is uniform across the

square-well confining potential. Schrödinger's equation, $H|\Psi\rangle = E|\Psi\rangle$, is now solved using the CI method. The N-electron wave function $|\Psi\rangle$ has the form

$$|\Psi\rangle = \sum_{I=0} c_I |\phi_I\rangle = c_0 |\phi_0\rangle + c_1 |\phi_1\rangle + c_2 |\phi_3\rangle + \cdots, \quad (5)$$

where $|\phi_I\rangle$ is the Ith Slater determinant and I ranges over all possible Slater determinants (configurations).

In general CI uses a variational wave function $|\Psi\rangle$ that is a linear combination of Slater determinants built from a complete set of orbitals. In the present work we have used Kohn-Sham orbitals, obtained self-consistently in the local-density approximation,[27,28] as the basis set. Following a convention similar to that of Szabo and Ostlund,[21] the N-electron wave function $|\Psi\rangle$ in this basis set can be written as

$$|\Psi\rangle = c_0 |\phi_0\rangle + \sum_{ra} c_a^r |\phi_a^r\rangle + \sum_{a<b,r<s} c_{ab}^{rs} |\phi_{ab}^{rs}\rangle + \cdots, \quad (6)$$

where $|\phi_0\rangle$ is the ground-state Slater determinant, constructed from the orbitals and obtained self-consistently using SDFT. Other determinants are described by how they differ from this $|\phi_0\rangle$. According to the convention, in $|\phi_0\rangle$, $a, b, c, \cdots$ are the occupied single-particle orbitals, while $r, s, t, \cdots$ are the unoccupied orbitals. Thus $|\phi_a^r\rangle$ is the singly excited determinant ("singles"), that is, a Slater determinant formed by exciting one electron from the single-particle orbital a to r. Similarly, the doubly excited determinant ("doubles") $|\phi_{ab}^{rs}\rangle$ is a Slater determinant obtained by exciting two electrons from occupied orbitals a and b to unoccupied orbitals r and s, respectively.

The actual calculation is carried out in two steps. First we obtain a set of single-particle orbitals by solving the Kohn-Sham equations self-consistently. This basis set contains both the occupied and the unoccupied orbitals. Second, we truncate the number of single-particle orbitals, obtained from earlier step, and generate a CI expansion using a recently developed CI method employing a numerical basis set of SDFT orbitals.[29] Further we also fix the S_z value for the system (that is, the number of up and down electrons), thereby fixing the number of possible Slater determinants (configurations). Thus, as an example, for a four-electron quantum dot we need three sets of calculations with $S_z = 0$, 1, and 2. Once we have a given set of orbitals (and configurations) we carry out the full CI expansion, where we take all possible excitations into account.

Our choice of DFT orbitals over conventional Hartree-Fock (HF) orbitals as the basis set is motivated by the ease with which the orbitals are generated. However, it should be noted that when we use DFT orbitals, the conventional rules of the Brillouin theorem (which states that[21] the singly excited determinants $|\Psi_a^r\rangle$ will not interact directly with the reference determinant $|\Psi_0\rangle$) are not applicable. Our preliminary studies have shown that the DFT basis is comparable to the HF basis and far better than a noninteracting single-particle basis.

The internal spin structure of the dot is analyzed using the spin-spatial pair-correlation function $g_{\sigma\sigma'}$. The function $g_{\sigma\sigma'}(\mathbf{r},\mathbf{r}')$ is proportional to the probability of finding an electron with spin z-component σ' at the position $\mathbf{r}'$ given

TABLE I. Convergence of energies (in Ha*) for two- and four-electron quantum dots in two sections of the table. In each sections the first row indicate the number of orbital considered for CI expansion and second row shows the number of configurations generated out of corresponding orbitals.

$N=2$; $S_z=0$					
Single particle orbitals	20	30	40	50	60
Configurations	400	900	1600	2500	3600
Energy ($r_s\sim8$)	0.2121	0.2120	0.2120	0.2120	0.2120
$N=4$; $S_z=0$					
Single particle orbitals	10	15	20	25	30
Configurations	2025	11025	36100	90000	189225
Energy ($r_s\sim8$)	0.6244	0.6219	0.6203	0.6201	0.6201

that another electron of spin σ is present at $\mathbf{r}$. It may be defined as

$$g_{\sigma\sigma'}(\mathbf{r},\mathbf{r}') = \langle\Psi|\hat{G}_{\sigma\sigma'}(\mathbf{r},\mathbf{r}')|\Psi\rangle, \quad (7)$$

where $\hat{G}_{\sigma\sigma'}(\mathbf{r},\mathbf{r}')$ is the two-body correlation operator given in configuration space by

$$\hat{G}_{\sigma\sigma'}(\mathbf{r},\mathbf{r}') = \sum_{i\neq j} \delta(\mathbf{r}_i-\mathbf{r})\delta(s_i-\sigma)\delta(\mathbf{r}_j-\mathbf{r}')\delta(s_j-\sigma'), \quad (8)$$

with $\mathbf{r}_i$ as the position and s_i as the spin variable (up or down) of electron i. The many-body wave function $|\Psi\rangle$ is given in the CI representation by Eq. (5). In the paper we consider $\mathbf{r}$ as the fixed position of a reference electron with spin σ and the correlation function is conventionally plotted as a function of the position and spin $(\mathbf{r}',\sigma')$ of the second electron. Thus, the first index of $g_{\sigma\sigma'}$ indicates the spin of the reference electron, which is fixed at the position $\mathbf{r}$. We also define the charge-charge correlation function as the spin-summed pair-correlation function,

$$g_\tau = \sum_{\sigma\sigma'} g_{\sigma\sigma'}. \quad (9)$$

A. Convergence

In all the CI calculations we test the convergence of energies, densities, and correlation functions as a function of the number of orbitals taken in the single-particle basis set. Table I shows the convergence of energies for two- and four-electron quantum dots for a typical low-density regime ($r_s \sim 8$). The table shows the number of orbitals taken in the CI expansion, resulting configurations, and corresponding energies. It can be seen that for the two-electron system 1600 configurations (40 orbitals) are sufficient to converge the energy to within ~0.1 mHa*($\sim10^{-7}$ eV). The equivalent convergence for $N=4$ quantum dot requires at least 90 000 configurations (25 orbitals).

It is also interesting to determine the number of dominant determinants (N_D) required to construct more than 99% of the densities and correlation functions. We do that by sorting

the coefficients (c_I^2) of the determinants of CI ground-state eigenvector.

Figure 1 shows a typical $g_{\uparrow\uparrow}$ correlation function for $N=4$, $S_z=1$ quantum dot at $r_s \sim 8$. The function is plotted along the diagonal of the well for four different values of N_D, namely, $N_D=1$, 10, 100 and using all determinants (i.e., 57 500 in this particular case). It can be seen that the difference between the correlation function with $N_D=100$ and with $N_D=$all is hardly noticeable. Thus it may be concluded that as few as 100 most dominant determinants successfully produce the correlation function. A similar convergence is also observed for the other correlation function and also for density. Thus in general only the first few hundred dominant Slater determinants are required to construct more than 99% of correlation functions and densities.

Further we would like to mention that the conventional HF-type determinant (where the lowest possible orbitals are occupied) may not be the most dominating determinant. We observe the contribution of the HF-type determinant to the total charge density in high- and low-density regimes. Table II shows such contributions for the four-electron quantum dot with and without impurity. In the high-density regime the
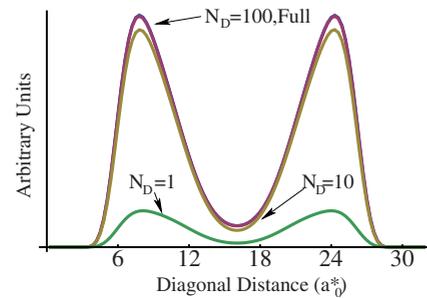
FIG. 1. (Color online) The $g_{\uparrow\uparrow}$ correlation function generated with four different values of terms. The functions are plotted along the diagonal for four-electron quantum dot ($S_z=1$) at $r_s \sim 8$. The reference electron is on the other diagonal line toward the corner (not shown here). Here $N_D=1$ means the correlation function with one Slater determinant and so on. It can be seen that the difference between the correlations with all the determinants ($N_D=$full) and that with only 100 terms is so small that it is beyond the resolution of the graph.

TABLE II. The contribution of HF determinant to the total charge density of the four-electron quantum dot. Observe that in presence of impurity the contribution reduces to 0.18%

	$r_s \sim 1.5$ (%)	$r_s \sim 4$ (%)	$r_s \sim 8$ (%)
Without impurity	~ 84	~ 17	~ 1.2
With impurity	~ 89	~ 2.5	~ 0.18

HF-type determinant is the most dominant and 80%–90% of the charge density is obtained only using this single determinant. However, with increasing r_s, its contribution diminishes to $\sim 1\%$ because of increasing correlations in the system.

III. RESULTS AND DISCUSSION

A. Pure system

Although our main emphasis in the paper is on the impurity effects, to put the results in proper perspective we first present the results for the pure system. We will also compare these results with those obtained by our earlier SDFT calculations[9] wherever applicable.

We consider the four-electron quantum dot as a representative case, for which $S^2=1$, $S_z=1$ (i.e., three up and one down electrons) is the ground state throughout the range of the sizes studied. Figure 2 shows the total charge density for two values of r_s, namely, $r_s=1.5$ (high density) and $r_s=8$ (low density).

In the high-density regime [Fig. 2(a)], the charge density is distributed throughout the well with four humps at the
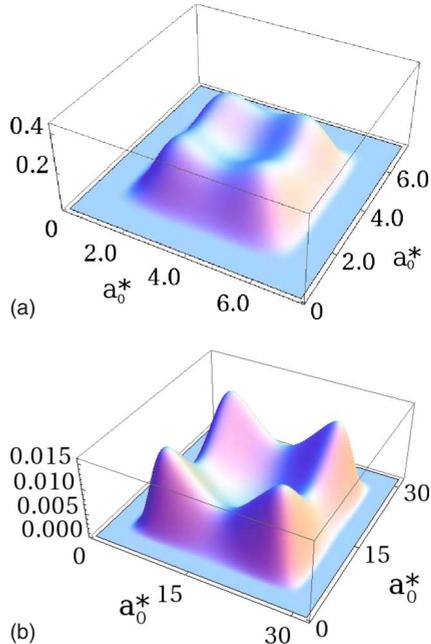
FIG. 2. (Color online) The total charge density $((a_0^*)^{-2})$ of four-electron ($S_z=1$) quantum dot for (a) $r_s=1.5$ and (b) $r_s=8$. The four prominent peaks in the low-density regime will eventually evolve into the localized peaks of a Wigner-molecule-like state.
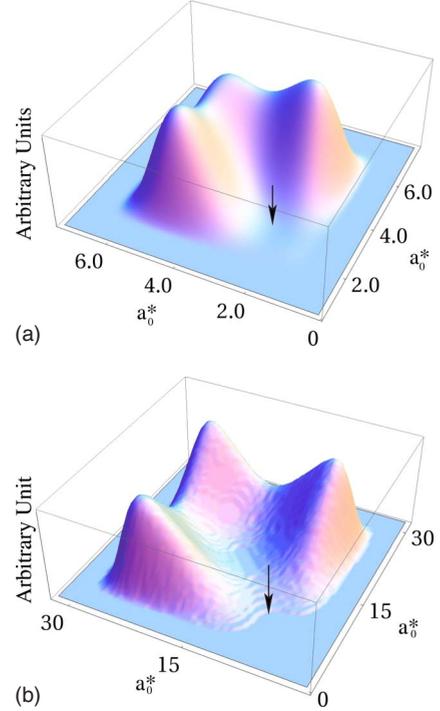
FIG. 3. (Color online) The pair correlation $g_{\uparrow\uparrow}$ is plotted for $N=4$ ($S=1$, $S_z=1$) in (a) high density ($r_s=1.5$) and (b) low density ($r_s=8$). The arrows show the position of reference electron.

corners. This is the well-known "Fermi-liquid" regime where the electrons have high kinetic energy. As the dot expands in size (that is, the density is lowered) the electrons lose their kinetic energy and begin to localize owing to the Coulombic repulsion, ultimately giving rise to the *Wigner-molecule-like* state in the limit of large r_s.[3,9,30–35] The beginning of the formation of such a state can be seen in Fig. 2(b), where the emergence of four localized corner peaks is clearly seen. In going from $r_s=1.5$ to $r_s=8a_0^*$, the peak-to-valley ratio of the charge density increases from about 1.8 to about 20. Such a transition from delocalized charge density to a more localized charge density is also seen from $N=2$ to $N=6$ electron quantum dots. It may be noted that such transitions were also seen in the SDFT studies[9] and SDFT results have qualitatively shown the correct nature of the charge density.

To understand the spin distributions in the dot we analyze the correlation functions $g_{\sigma\sigma'}$. Figure 3 shows the $g_{\uparrow\uparrow}$ pair correlation for the high- and low-density regimes. The position of the reference electron is marked by an arrow. In $g_{\uparrow\uparrow}$ the absence of correlation function at the position of the reference electron illustrates the exchange hole. Further we plot the spin density, which is defined to be the difference between the up and down charge densities, i.e., $(\rho_\uparrow - \rho_\downarrow)$. Figure 4 shows the spin density for the four electron dot at $r_s \sim 8$. We recall that there are three up and one down electrons in the system, giving $S_z=1$. The inspection of the spin density in Fig. 4 shows that the net spin is thus distributed equally on the four corner peaks.

We note that, since SDFT has the form of a mean-field theory, it has limitations in the correlated region. The low-density region (i.e., $r_s=8$) is the region where the correlations are significant and the CI method shows a substantial
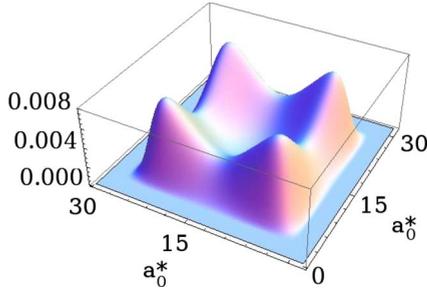
FIG. 4. (Color online) The spin density ($\rho_\uparrow - \rho_\downarrow$) for four-electron (three up and one down) dot at low density shows that the excess spin is clearly distributed on the four peaks.

difference in the amount of localization. To illustrate the point, we plot the total charge density along the diagonal of the square well for the high- and low-density regions using SDFT and CI, which is shown in Fig. 5. It can be seen from the figure that in the high-density regime the SDFT and CI charge densities are nearly identical. However, in the low-density regimes the CI density can be seen to be sharper than those of SDFT. The peaks of the CI density are about 20% higher than SDFT, showing more localization of density. In general, for the systems under investigation, SDFT underestimates the localization effects seen in correlated regimes.

1. Inhomogeneities in correlations

In a recent work, Ghosal *et al.*[14] have studied the effects of correlations on the circular quantum dot using the diffusion quantum Monte Carlo technique (for up to 20 electrons). They showed that the increasing electron-electron interaction leads to angular inhomogeneities in the charge
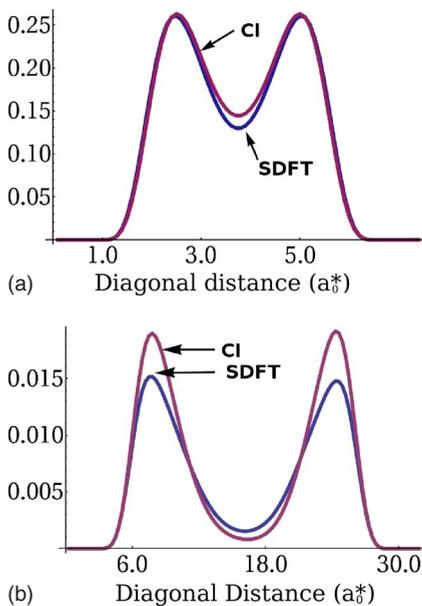
FIG. 5. (Color online) The total charge densities ($(a_0^*)^{-2}$), plotted along the diagonal of the well, for four-electron quantum dot. The densities are plotted for two different densities, (a) $r_s \sim 1.5$ and (b) $r_s \sim 8$, using CI and SDFT methods. At low densities it is evident that SDFT underestimates the localization.
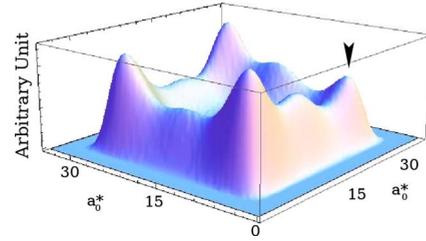
FIG. 6. (Color online) Charge-charge correlation for $N=5$ ($S_z = 1/2$, $r_s = 8$) shows the formation of small inhomogeneous humps along walls of the quantum dot. (The arrow shows the position of the reference electron.)

density. They have attributed such inhomogeneities to correlation effects.

To analyze such inhomogeneities, we examine the five-electron quantum dot in low-density regime ($r_s \sim 8$), where the correlation effects are more dominant. Figure 6 shows the charge-charge correlations g_τ for the same quantum dot. The clear oscillatory pattern is also seen in the spin-spatial pair correlations. It is clear that correlation-induced inhomogeneities are also seen at such low electron count and are a generic feature of quantum dots.

2. Excited states

One of the advantages of using the CI method over other methods such as Monte Carlo is that it provides access to the excited states of the system. This has been harnessed by a variety of authors for a variety of systems including quantum dots. Reimann *et al.*[31] studied the excited states of a parabolic quantum dot in the Wigner localization regime. They have examined the eigenvalue spectra of a six-electron quantum dot as a function of r_s and analyzed the evolution of the same. They have observed that the fully polarized state of the six-electron parabolic quantum dot moves substantially closer to the unpolarized ground state, although they do not observe any crossing of the two. In a recent interesting experiment Kalliakos *et al.*[20] observed *rotovibrational* modes indicating that the such molecular excitations develop on the onset of short-range correlations occurring even at $r_s \sim 1.71$.

We discuss the excited states with the example of the two-electron quantum dot. Figure 7 shows the first ten eigenvalues for a two-electron quantum dot (spin-singlet ground state) in three different density regions, namely, $r_s \sim 1.5$, $r_s \sim 5$, and $r_s \sim 14$. The figure also shows the total spin quantum number S of the individual states. A double notation such as "0, 0" or "1, 1" indicates a doubly degenerate $S=0$ or 1 state, respectively. In all the density regimes, the ground state of the dot remains a spin singlet, as expected.

It should be noted that as r_s increases the eigenspectrum becomes compressed. For instance, the spread of the first ten eigenvalues in Fig. 7 changes from 1.98 Ha* ($r_s = 1.5a_0^*$) to 0.024 Ha* ($r_s = 14a_0^*$). This is because in the low-density regime the electrons lose their kinetic energy and the dominant energy is Coulombic. The ordering of the spins and degeneracies shown in Fig. 7 changes as r_s increases, implying that there have been level crossings or anticrossings as r_s changes. For example, while the first-excited level remains a
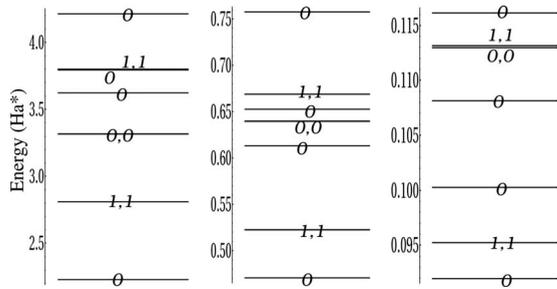
FIG. 7. Eigenvalue spectra of a two-electron quantum dot shown in three density regimes: (a) high density ($r_s \sim 1.5$), (b) intermediate density ($r_s \sim 5$), and (c) low density ($r_s \sim 14$). The total spin quantum number S of the corresponding state is shown; a double notation such as 0, 0 indicates a pair of degenerate levels. Note that the energy scales of the three regimes are different.

doubly degenerate triplet, a doubly degenerate singlet moves from being the second excited level at $r_s = 1.5a_0^*$ to the third excited level at $r_s = 5a_0^*$ and the fourth excited level at $r_s = 14a_0^*$.

The effect of Coulombic interaction can also be seen in the charge densities. We plot the charge densities of the excited states for the same system ($N = 2$, $S_z = 0$) in Fig. 8. The left-hand panel of the figure shows the first few excited states from the high-density region ($r_s \sim 1.5$), while the right-hand panel shows those from the low-density region ($r_s \sim 14$). The topmost row, which is the ground state of the system, clearly shows the transition from Fermi liquid to a more localized state, as discussed earlier.

It is interesting to observe the nature of the charge densities for the first and second excited states in the high-density regime (second and third rows of the left-hand panel of Fig. 8). The first and second excited states are degenerate and together they follow the rotational symmetry of the well. A peculiar case is that of the localization along the wall only as seen in the seventh excited state [Fig. 8].

However, while the high-density regime shows a variety of charge distributions and nodal structures, in the low-density regime the charge densities of the first several excited states are all very similar to that of the ground state and consist of four humps near the four corners of the square well. This feature can be understood qualitatively as a consequence of the localization of the electrons.

On the basis of the detailed symmetry adopted CI calculations it has been noted by Kalliakos *et al.*[20] that for low densities the low-lying excited states of parabolic quantum dot can be described by a rigid rotator. An analogous idea should apply here, except that the notion of rotational states must be modified to take account of the fourfold rather than continuous rotational symmetry. Nevertheless, it is reasonable to expect that the first few low-lying states should all have the same underlying localization pattern but differ only in terms of the various rotational quantum numbers that are appropriate for the system. Interestingly, in the square-well case, the pattern of the localization is seen to be strongly influenced by the geometry of the confining potential. This feature at low density is a general feature and can be seen for all the systems under investigation ($N = 2$ to $N = 6$ electron quantum dots).

B. Impurity in the quantum dot

We now examine the effects of an impurity on the quantum dot and contrast these results with the pure system. Figure 9 shows the ground state ($S^2 = 1$, $S_z = 1$) charge densities for $N = 4$ electron system for the high- and low-density regions [Figs. 9(a) and 9(c)]. For the sake of clarity, the zoom of the lower part of the figure is shown in the right-hand panel [Figs. 9(b) and 9(d)].

It is evident from Fig. 9 that the presence of the attractive potential has modified the charge density significantly by accumulating the charge at the center. Note that the small humps seen in the high-density regime will eventually localize to form Wigner-molecule-like systems in the low-density regime.

The parameters of the impurity are such that in the low-density regime there is always one unit of charge around the impurity site. (The charge inside the impurity is calculated by constructing a circle of radius r centered on the impurity and integrating the charge inside it, where r is taken to be of the order of the width of the impurity.) Thus the central peak of the charge density is due to the impurity and the charge outside the impurity site undergoes the transition from a delocalized to a localized state. However, the presence of charge at the impurity site pushes the remaining charge outward making it more localized and sharper than in the pure case.

The effect of the impurity can be analyzed further by means of the correlation functions. Figure 10 shows the pair-correlation functions $g_{\uparrow\uparrow}$ and $g_{\uparrow\downarrow}$ for a four-electron quantum dot in two different density regimes. Let us recall that the calculation is for three up and one down electrons and the up electron is the reference electron, which is fixed at the center of the dot (at the impurity site).

The up-up correlations $g_{\uparrow\uparrow}$ show a void at the center irrespective of the dot size, which is just the *exchange hole* due to the Paul exclusion principle. The pair function $g_{\uparrow\uparrow}$ also shows the higher degree of localization in the low-density regime, which is expected. As seen from Fig. 10, while the up-up correlation remains qualitatively unchanged as a function of r_s, the up-down correlation has a different character.

In the high-density regime, one sees a prominent peak in $g_{\uparrow\downarrow}$ around the impurity (Fig. 10). This is the density regime where electrons have high kinetic energy and electrons in the well can overcome the Coulombic repulsion to overlap with the impurity site. The correlation function peaks at the impurity site and is dominated by the impurity potential.

On the other hand, as the dot size increases, the central spin-down electron is expelled from the impurity site owing to the Coulomb correlations and localizes on the corners of the well. As a consequence, the impurity site progressively acquires a net magnetic moment due to the presence there of just a single electron. This is reflected in the up-down correlations of the low-density regime by the absence of the correlation function at the reference cite. It may be noted that the impurity site changes from nonmagnetic to completely magnetic as r_s increases. This result is general and holds good for the dot containing six electrons also.

An interesting observation to be noted from Fig. 10 is that in the low-density region the up-up and the up-down corre-
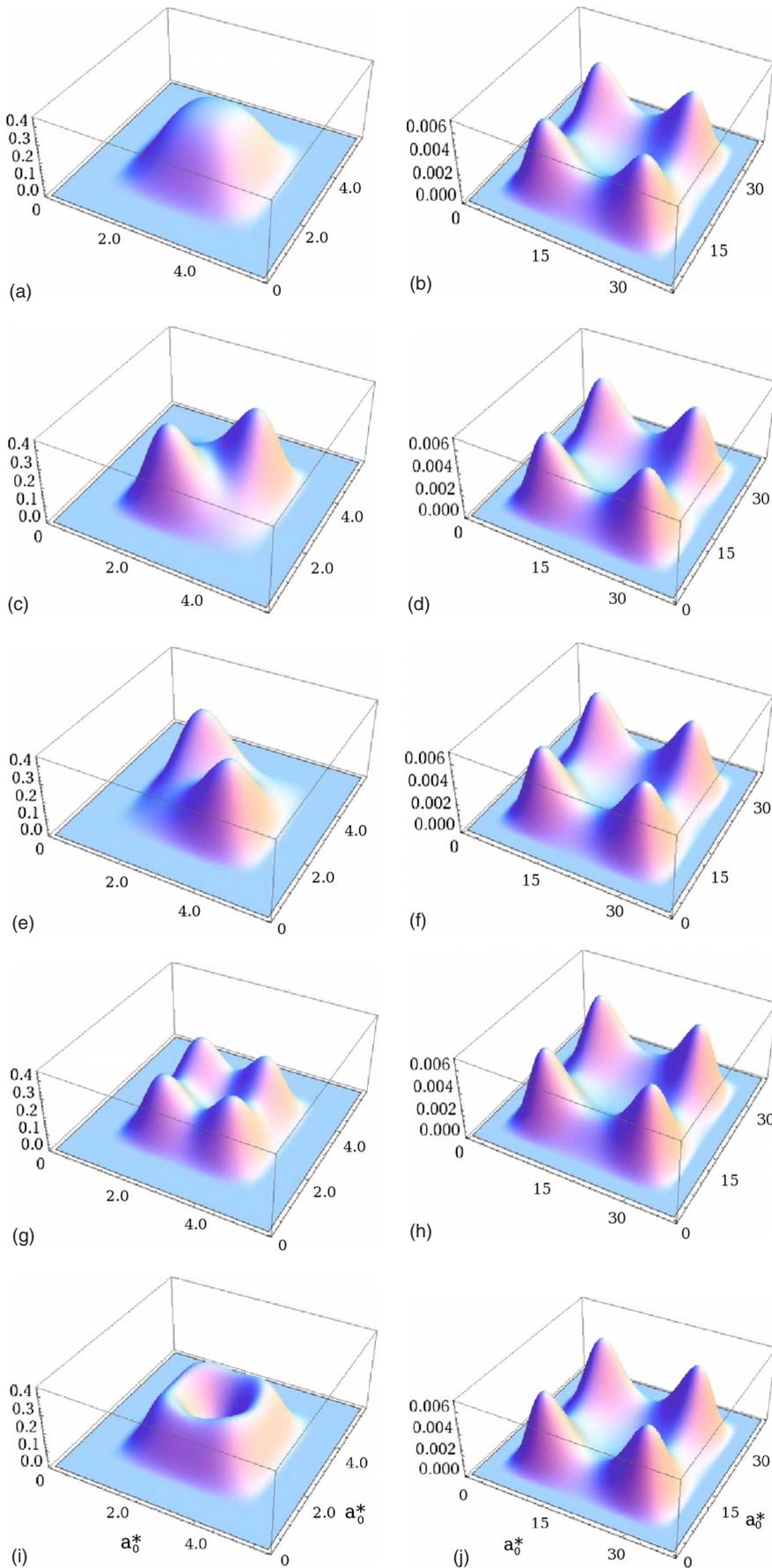
FIG. 8. (Color online) Total charge density $((a_0^*)^{-2})$ of excited states of two-electron quantum dot $(S=0, S_z=0)$. Left-hand panel shows the excited states in high-density regime and the right-hand side shows that in low-density regimes. (a), (b) Ground state; (c), (d) first excited state; (e), (f) second excited state; (g), (h) fifth excited state; (i), (j) seventh excited state. In the low-density regime the states can be seen to have almost identical charge density.
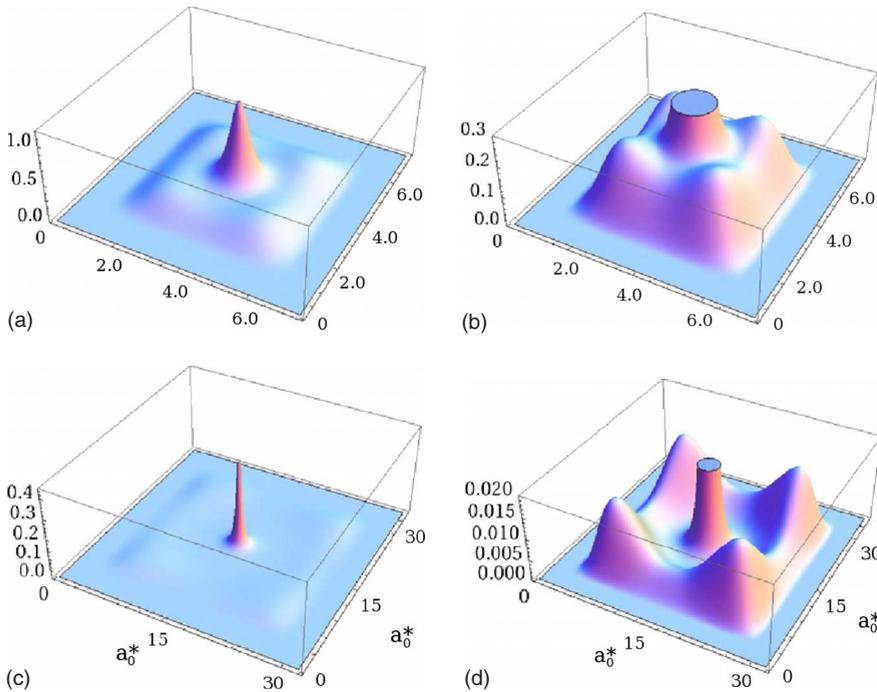
FIG. 9. (Color online) The total charge density $((a_0^*)^{-2})$ for $N=4$, $S_z=1$ quantum dot is shown. The upper row shows the charge density at $r_s \sim 1.5$ with bottom section zoomed on right side. Similar picture for low charge density $(r_s \sim 8)$ regime is shown in the lower row.

lations appear qualitatively similar. This can also be regarded as the effect of the domination of the Coulombic energy over other contributions to the energy, including the exchange interaction. In such a low-density regime, the eigenspectrum is nearly degenerate, which makes it difficult to determine the exact S^2, S_z state of the ground state for large values of r_s.

It is instructive to analyze the nature of the magnetic ordering in the quantum dots as a function of number of electrons. In the high-density regime, there is no magnetic order, in the sense that the spin density is everywhere zero for $S_z=0$, while for $S_z \neq 0$ it follows the charge density. On the

other hand, in the low-density regime, the localized peaks acquire a net magnetic moment depending upon the number of electrons, as we now discuss.

The two-electron quantum dot $(S=0, S_z=0)$ has one up and one down electrons and shows very interesting nature in low density. We have calculated and examined the spin-correlation function $g_{\uparrow\downarrow}$, with the reference electron (say up) at the center of the dot. Correlation function shows identical features as seen for four-electron case [Fig. 10(d)], namely, zero value around the center and the four distinct peaks at the corners. Evidently in this region, if the up electron is local-
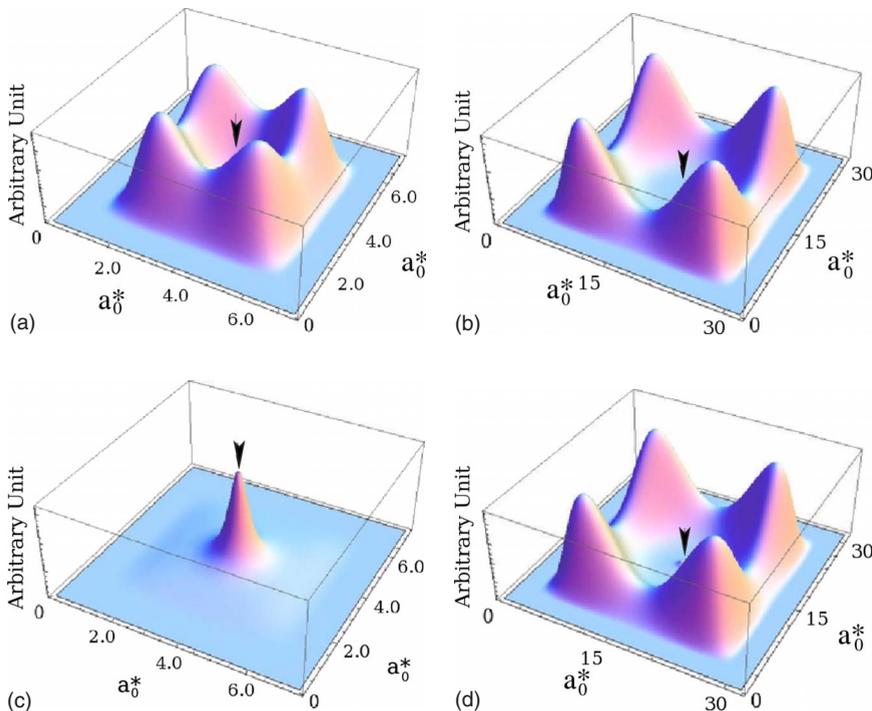
FIG. 10. (Color online) $g_{\uparrow\uparrow}$ and $g_{\uparrow\downarrow}$ correlations for four-electron quantum dot in two different density regimes. The reference electron is located at the center of the dot and is marked with the arrow. Observe the drastic change in the behavior of $g_{\uparrow\downarrow}$. The impurity site changes its nature from nonmagnetic to magnetic as the size of dot is changed.
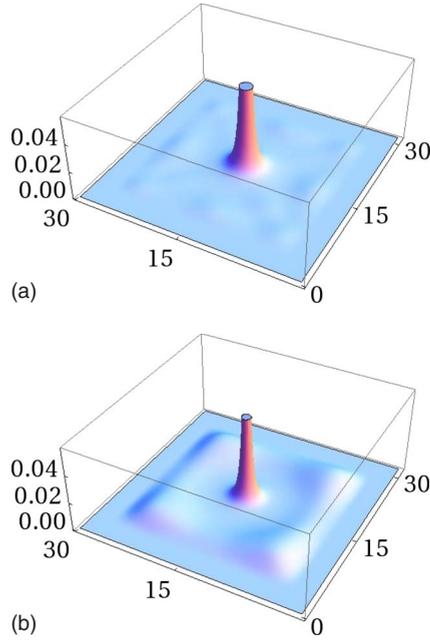
FIG. 11. (Color online) Spin-density plots for (a) $N=3$ and (b) $N=4$. The central peaks are cropped for the sake of clarity. Observe that in both the cases the central site is occupied by the one up electron resulting in sharp peak seen. For three-electron case the spin density is numerically zero everywhere else. On the other hand, for four-electron case all the four corners of the well have the net up magnetic moment of $(1/4)\mu_B$.

FIG. 12. Eigenvalue spectra of the two-electron quantum dot with impurity for three density regimes, namely, $r_s \sim 1.5$, 8, and 14. The number next to the states indicates the total spin quantum number S. A double notation 0, 0 or 1, 1 denotes a pair of degenerate levels with the indicated spin, while "0, 1" denotes a pair of nearly degenerate levels (see text). There is a clear bunching of $S=0$, 1 pairs in low-density regimes. Such a feature was absent in the pure case (no impurity).

ized on the impurity, then the down electron forms four localized peaks near the corners of the well. Thus each of these external peaks carries $(1/4)\mu_B$ in the opposite direction to the impurity moment. The outer peaks now have an antiferromagneticlike coupling to the impurity.

On adding a third electron to the system, one finds a ground state with two up and one down electrons ($S_z=1/2$), with the up electron trapped at the impurity and as a consequence a net zero magnetic moment (spin compensation) on the outer peaks. This is illustrated in Fig. 11(a). The figure shows the spin density for $N=3$, where the sharp peak is due to the trapped electron and the zero-spin density everywhere else depicts the spin compensation.

Adding one further electron results in a four-electron quantum dot, which has three up and one down electrons in its ground state ($S=1$, state with maximum $S_z=1$). Figure 11(b) shows the spin density for this case. This extra spin-up electron is distributed on the localized peaks resulting in a net spin-up magnetic moment of $(1/4)\mu_B$ on each peak.

The system thus tends to have the distribution for the ground state which minimizes the total magnetic moment on the external peaks. This holds true also for the quantum dot with $N=5$ (three up and two down), where the external peaks have zero magnetic moment. Similarly, for the six-electron quantum dot, the external peaks have a net down magnetic moment of $(1/4)\mu_B$. Thus, as a function of the number of electrons, the magnetic moment on the four external peaks fluctuates. It is worth pointing out that for $N=2-6$ it is always the up electron that is trapped at the impurity site in the ground state with maximum S_z.

1. Comparison of SDFT and CI

At this stage it is worth comparing the SDFT results[9] with those obtained by CI. It should be noted that the qualitative picture of total charge density emerged out of SDFT is correct even in case of impurity. In many cases the SDFT is able to show the antiferromagneticlike coupling seen in CI. However the amount of localization differs as shown in Fig. 5. Upon introduction of the impurity the SDFT tends to show several broken-symmetry states, while CI produces symmetry-preserved solutions, as expected. Unlike SDFT, the CI approach also provides the ability to probe the excited states of the system, which we shall present in Sec. III B 2.

2. Excited states

We now discuss the effect of an impurity on the excited state of the system. Figure 12 shows the evolution of the eigenvalue spectrum as a function of r_s. If we compare the nature of the eigenvalue spectrum in the high-density regime with that of pure case, we notice that the structure is largely unchanged, although the spectrum itself is lowered in energy because of the presence of attractive potential at the center.

However, as r_s increases, the effect of the impurity becomes significant. Two striking features emerge. First, the doubly degenerate states, whether spin singlet or triplet, move up in the spectrum as r_s increases and the lowest-lying states consist of nondegenerate states only. Second, pairs of states with $S=0$ and $S=1$ become nearly degenerate. In the extremely low-density regime there is hardly any overlap among the electronic wave functions of the localized electrons. In consequence, the exchange interaction becomes very small. The singlet-triplet splitting is thus reduced to such an extent that even the ground state is (nearly) degenerate with the first-excited state ($\Delta E \sim 1$ mHa*). The case of $r_s=8$ is intermediate with a weak singlet-triplet splitting observed in the ground state.

It is instructive to study the charge densities of corresponding eigenstates. Figure 13 shows two panels containing the charge densities of a few excited states of a two-electron quantum dot. The left-hand panel shows the densities from
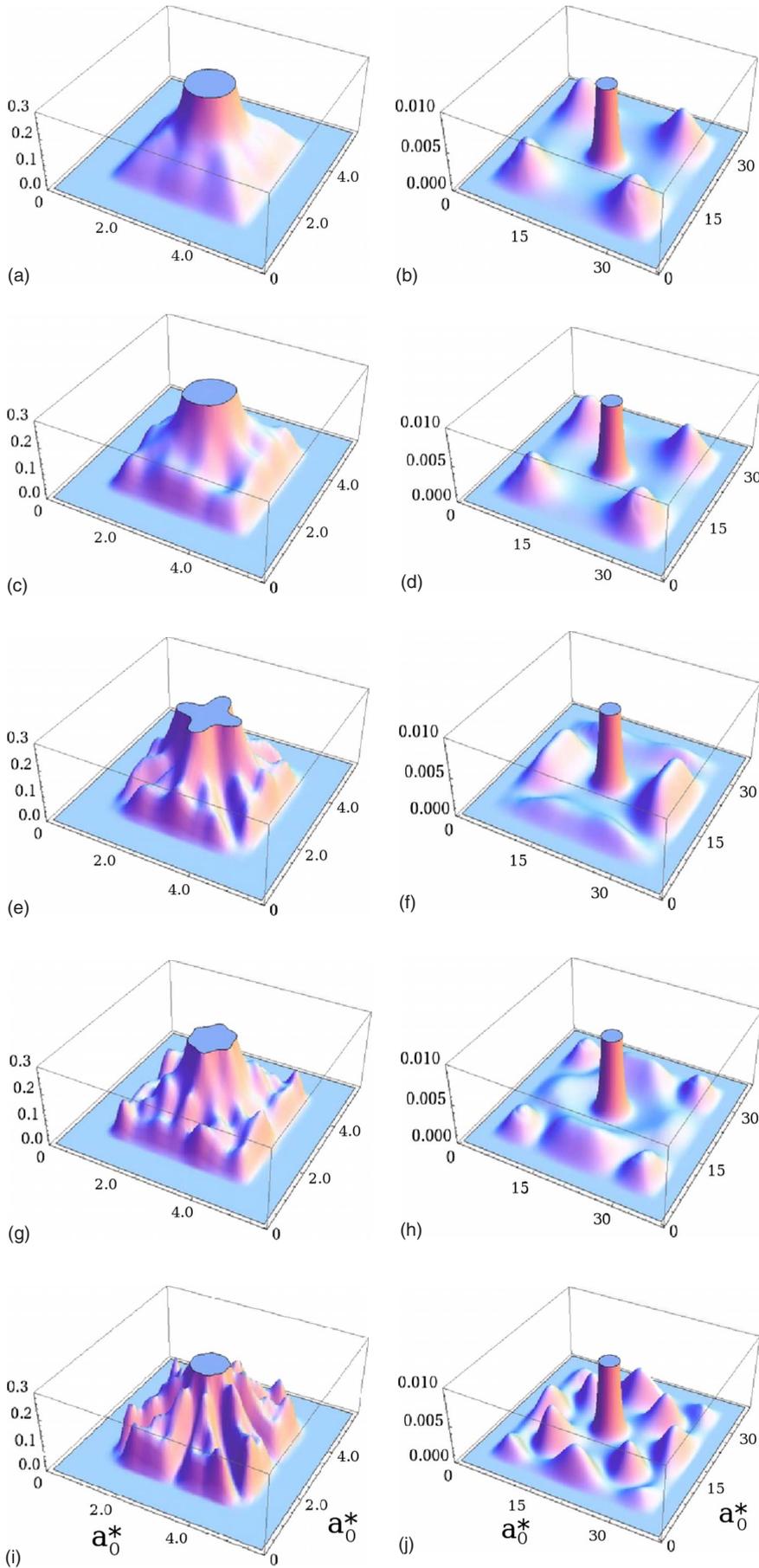
FIG. 13. (Color online) Total charge density $((a_0^*)^{-2})$ of excited states of two-electron quantum dot ($S=0$, $S_z=0$). The central peak is cropped for the sake of clarity. Left-hand panel shows high-density regime, while the right-hand panel shows the low density. (a), (b) Ground excited state; (c), (d) first excited state; (e), (f) fourth excited state; (g), (h) sixth excited state; (i), (j) eighth excited state. The single electron is trapped inside the impurity (at the center). The remaining electron displays a variety of charge distribution due to the nodal structure of the wave function.

high-density regime ($r_s \sim 1.5$) and the right-hand panel shows the same for the low-density ($r_s \sim 14$) regime. It should be noted that except for the ground state, the presence of level crossings means that the states shown in each row of the figure may not be adiabatically related to each other as r_s varies from high to low density. In all the figures, the peak of the impurity is cropped for the sake of clarity.

The high-density regime is clearly dominated by the presence of the impurity, which covers a substantial area. The charge density at high energy shows sharp features in the outer region (particularly the sixth and eighth excited states) that were absent in the pure quantum dot. Analogous features are present more clearly as side peaks in the low-density regime. To understand these side peaks, we recall that at low density one of the two electrons localizes into the impurity well, while the other remains outside. The low-lying excited states of the two-electron system at low density then correspond to the excited states of this outer electron, which moves in a net potential equal to the sum of the square-well confining potential and the Coulomb repulsion from the central electron. There is also a spin coupling between the central and outer electron, which as discussed above leads to nearly degenerate singlet and triplet states, $S=0$ and $S=1$. In the ground state ($S=0$) of the outer electron has four peaks (of charge $e/4$) symmetrically in each of the corners; the first-excited state is the $S=1$ coupling of the same one-electron states. Higher excited states of the outer electron show additional nodes. In the fourth excited state, the nodes follow an approximately ringlike pattern, located in the region between the outer hard-wall potential of the square well and the inner impurity electron. In higher states such as the eighth excited state, the nodal structure becomes two dimensional, that is, extending toward the center of the dot as well as around the walls. At high density (left-hand panel in Fig. 13), a less distinct version of these confinement peaks is also evident in the density near the edge of the well.

The nature of the excited states for the two-electron case is thus dominated by the nodal structure of the wave functions. However, we also note that this variation in excited states is unique to the $N=2$ case. With increased number of electrons, the total charge density of the lowest-lying states does not show such a distinctive feature.

IV. CONCLUSION

In this work we have investigated the electronic structure of square quantum dots containing an attractive impurity at the center. The calculation has been carried out for two to six electrons using the full CI technique. We have used the Kohn-Sham single-particle orbitals for the construction of the many particle wave function.

As expected, in the pure system we observe the beginning of the transition toward a Wigner-molecule-like state at low density. The effect of correlations is seen in the enhancement of the localization of charge densities ($\sim 20\%$) as compared to that obtained from SDFT calculations. We also find signatures of correlation-induced inhomogeneities as reported by Ghosal et al.[14] in their quantum Monte Carlo work. We also discussed the excited states of pure quantum dots.

Our correlation analysis shows that the character of the impurity changes from nonmagnetic to magnetic as the size of the dot is increased. At large r_s, a single spin-up electron is trapped in the impurity well. In this case, we observe the localized magnetic moments at five sites, namely, four corners and one impurity site. For the two-electron case, the surrounding (down) localized spins are coupled to the impurity in antiferromagnetic ordering.

The charge densities of excited states of the two-electron dot in the presence of the impurity show a variety of charge distributions. Such distributions can be understood in terms of the confinement effect on the outer electron, with the other electron localized at the impurity site.

Interestingly, we observe that only a small fraction (typically of the order of a few hundreds) of the total number of configurations (Slater determinants) contribute to properties such as the charge density and the correlation functions. In the strongly correlated regime, the contributions to the charge density and the correlation functions of the Hartree-Fock-type determinant, that is, obtained by occupying the lowest-energy states, are almost negligible.

The comparison of CI with SDFT shows that the qualitative nature of the results is well produced by the SDFT. However, in the strongly correlated regime, SDFT underestimates the localizations.

---

*bspujari@physics.unipune.ernet.in

[1] M. Reed, Sci. Am. **268**, 118 (1993).

[2] R. C. Ashoori, Nature (London) **379**, 413 (1996).

[3] S. M. Reimann and M. Manninen, Rev. Mod. Phys. **74**, 1283 (2002).

[4] S. Tarucha, D. G. Austing, T. Honda, R. J. van der Hage, and L. P. Kouwenhoven, Phys. Rev. Lett. **77**, 3613 (1996).

[5] D. G. Austing, S. Sasaki, S. Tarucha, S. M. Reimann, M. Koski-nen, and M. Manninen, Phys. Rev. B **60**, 11514 (1999).

[6] C. E. Creffield, W. Häusler, J. H. Jefferson, and S. Sarkar, Phys. Rev. B **59**, 10719 (1999).

[7] E. Räsänen, H. Saarikoski, M. J. Puska, and R. M. Nieminen, Phys. Rev. B **67**, 035326 (2003).

[8] S. A. Akbar and I. H. Lee, Phys. Rev. B **63**, 165301 (2001).

[9] B. Pujari, K. Joshi, D. G. Kanhere, and S. A. Blundell, Phys. Rev. B **76**, 085340 (2007).

[10] E. Räsänen, H. Saarikoski, V. N. Stavrou, A. Harju, M. J. Puska, and R. M. Nieminen, Phys. Rev. B **67**, 235307 (2003).

[11] C. Yannouleas and U. Landman, Phys. Rev. Lett. **82**, 5325 (1999).

[12] A. Harju, E. Räsänen, H. Saarikoski, M. J. Puska, R. M. Nieminen, and K. Niemelä, Phys. Rev. B **69**, 153101 (2004).

[13] W. M. C. Foulkes, L. Mitas, R. J. Needs, and G. Rajagopal, Rev. Mod. Phys. **73**, 33 (2001).

[14] A. Ghosal, A. D. Güçlü, C. J. Umrigar, Denis Ullmo, and Harold U. Baranger, Nat. Phys. **2**, 336 (2006).

[15] T. M. Henderson, K. Runge, and R. J. Bartlett, Chem. Phys. Lett. **337**, 138 (2001).

[16] I. Heidari, S. Pal, B. S. Pujari, and D. G. Kanhere, J. Chem. Phys. **127**, 114708 (2007).

[17] G. W. Bryant, Phys. Rev. Lett. **59**, 1140 (1987).

[18] M. Borgh, M. Toreblad, M. Koskinen, M. Manninen, S. Aberg, and S. M. Reimann, Int. J. Quantum Chem. **105**, 817 (2005).

[19] M. Rontani, C. Cavazzoni, D. Bellucci, and G. Goldoni, J. Chem. Phys. **124**, 124102 (2006).

[20] S. Kalliakos, M. Rontani, V. Pellegrini, C. Garcia, A. Pinczuk, G. Goldoni, E. Molinari, L. Pfeiffer, and K. West, Nat. Phys. **4**, 467 (2008).

[21] A. Szabo and N. Ostlund, *Modern Quantum Chemistry* (Dover, New York, 1996).

[22] E. Räsänen, J. Könemann, R. J. Haug, M. J. Puska, and R. M. Nieminen, Phys. Rev. B **70**, 115308 (2004).

[23] M. Şahin and M. Tomak, Phys. Rev. B **72**, 125323 (2005).

[24] J. L. Movilla and J. Planelles, Phys. Rev. B **71**, 075319 (2005).

[25] F. J. Ribeiro and A. Latgé, Phys. Rev. B **50**, 4913 (1994).

[26] B. Reusch and R. Egger, Europhys. Lett. **64**, 84 (2003).

[27] B. Tanatar and D. M. Ceperley, Phys. Rev. B **39**, 5005 (1989).

[28] P. Gori-Giorgi, C. Attaccalite, and S. M. G. B. Bachelet, Int. J. Quantum Chem. **91**, 126 (2003).

[29] K. Joshi and S. Blundell (unpublished).

[30] E. P. Wigner, Phys. Rev. **46**, 1002 (1934).

[31] S. M. Reimann, M. Koskinen, and M. Manninen, Phys. Rev. B **62**, 8108 (2000).

[32] A. Harju, S. Siljamäki, and R. M. Nieminen, Phys. Rev. B **65**, 075309 (2002).

[33] A. V. Filinov, M. Bonitz, and Y. E. Lozovik, Phys. Rev. Lett. **86**, 3851 (2001).

[34] B. Reusch, W. Häusler, and H. Grabert, Phys. Rev. B **63**, 113313 (2001).

[35] A. Ghosal, A. D. Güçlü, C. J. Umrigar, D. Ullmo, and H. U. Baranger, Phys. Rev. B **76**, 085341 (2007).